# A COMPARISON OF THE MECHANICAL PROPERTIES OF Fe-Cr-Si-B METALLIC GLASS WIRES AND HT STEEL WIRES

J. A. Verduzco, R. J. Hand and H. A. Davies

Department of Engineering Materials, University of Sheffield
Mappin Street, Sheffield, S1 3JD, UK

## ABSTRACT

The mechanical properties of melt-spun of $Fe_{78-x}Cr_xSi_{10}B_{12}$ amorphous alloy wires are compared with those of HT steel wires. Fracture toughness was measured for melt spun ribbon. A new double-pulley tensioning machine has been developed to facilitate tension/compression fatigue testing of the $Fe_{78-x}Cr_xSi_{10}B_{12}$ amorphous alloys and the HT steel wires. Some tension/tension fatigue testing was also performed using a single pulley testing machine. The tensile strength and microhardness increased and the fatigue performance improved with the substitution of Fe by Cr. The fatigue performance of the glassy alloys was *generally* similar when expressed on the basis of bend strain but inferior when expressed on the basis of bend stress. Fracture toughness was largely independent of Cr content. Fractography revealed differences in the fracture surface features for the amorphous wires tested in the two different modes.

## INTRODUCTION

It is well known that the mechanical strengths of some Fe-based amorphous alloys produced in the rotating water bath melt spinning process [1] are higher than those of high tensile (HT) steel wires [2,3]. It is difficult to measure the mechanical properties of very fine amorphous wires by conventional methods and thus novel methods have been developed to study and to analyse them (see, for example [3,4]). It has been found that the fatigue limit for the Fe-Cr-Si-B quaternary alloy system increases on replacing Fe by Cr, reaching a maximum at 10 at% Cr; above this Cr content the as-cast wires are brittle rather than ductile. The enhancement in the fatigue limit has been attributed to the formation of a protective film composed of Cr/Si hydrated oxide. These enhancements in fatigue properties were observed using tension/tension testing only. In this paper we consider the behaviour of the $Fe_{78-x}Cr_xSi_{10}B_{12}$ compositional series under tension/compression and tension/tension loading. Microhardness, tensile strength and fracture toughness measurements have also been undertaken; for practical reasons the latter tests were conducted on ribbons rather than wires.

## EXPERIMENTAL

Glassy alloy wires (diameter 90 to 130 $\mu m$), from the compositional series $Fe_{78-x}Cr_xSi_{10}B_{12}$, ($0 \leq x \leq 8$), were directly cast using a rotating water bath melt spinning process, similar to that described by Onhaka [1]. The wires were fully bend ductile and x-ray diffractometry (Co K$\alpha$ radiation) confirmed that they were amorphous. HT steel wires tested were standard brass plated tyre reinforcement filament (245 $\mu m$ diameter) supplied by Goodyear, Luxembourg. Vickers microhardness tests were performed on the wires before and after fatigue tests using an indentation load of 100 *g* for 20 *s*; around 50 measurements were used in each case in order to determine the average microhardness. Tensile tests were performed on a Hounsfield tensometer at a strain rate of $1x10^{-4}\ s^{-1}$; a Camscan S2 Scanning Electron

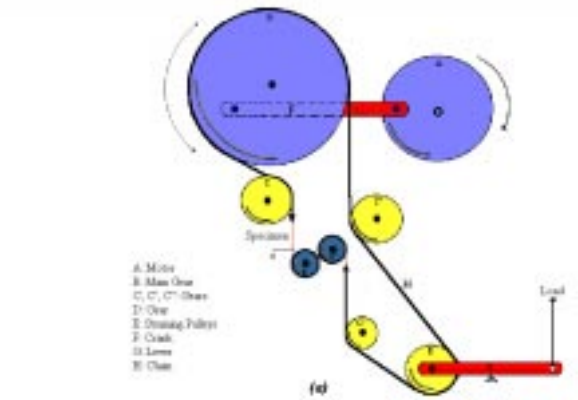

**Figure 1.- Schematic illustration of the new twin pulley fatigue testing machine.**

Microscope (SEM) was used to determine the cross sectional area at fracture in each case in order to calculate the ultimate tensile strength.

Fatigue tests on wires of the $Fe_{78-x}Cr_xSi_{10}B_{12}$ alloy series were carried out using both an existing single pulley bend type fatigue testing machine [3] (SP) which produces only tension/tension loading and a modified fatigue machine which uses two pulleys (DP) which can perform tension/compression loading, figure 1. To facilitate comparison between the two testing machines, the single pulley tests were carried out using a constant mean stress of 1550 MPa rather than the constant minimum stress utilised previously [3,5]. The double pulley tests were carried out at constant mean stresses of 200, 900 and 1550 MPa. The HT steel wires were tested in the DP machine at a constant mean stress of 200 MPa. The load frequency for all the fatigue tests was 3.4 *Hz* and the tests were carried out in ambient humidity (RH~60%). The stress range, $\Delta\sigma_a$, experienced by the outer surface of the bent wire sample in the SP machine is given by:

$$\Delta\sigma_a = E \cdot \frac{d_w}{d_w + d_p} \tag{1}$$

where $E$ is the Young's Modulus (extrapolated from Donald *et al* [6]) and $d_w$ and $d_p$ are the wire and pulley diameters, respectively. Thus, for equivalently sized pulleys the stress range in the DP machine is twice that in the SP machine. Figure 2 shows schematically the surface stress profile generated by each machine.

In order to determine the fracture toughness for glassy metallic alloys, ribbons of thickness ~45 $\mu m$ were cast using the chill block melt spinning quenching technique at a roll speed ~30 $ms^{-1}$ under an atmosphere of

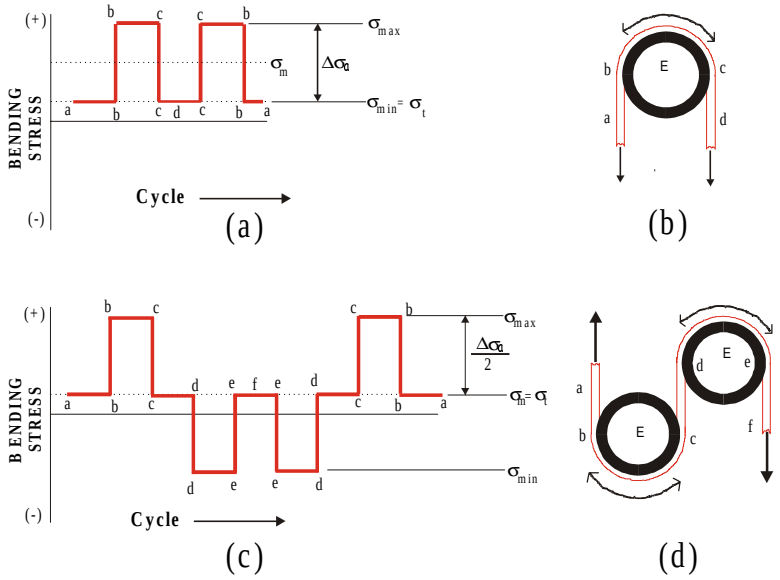


**Figure 2.- Schematic illustration for the surface bending stress cycles for the single (SP) (a) and (b), and double (DP) (c) and (d) pulley machines; where $\Delta\sigma_a$, $\sigma_m$, $\sigma_t$, $\sigma_{min}$ and $\sigma_{max}$ are the stress range, mean stress, tensioning load, minimum and maximum stresses respectively.**

helium. A notch was cut in the ribbons which were tested at a strain rate of $1.66 \times 10^{-4}\ s^{-1}$ in a Hounsfield tensometer. The fracture toughness was obtained from the resultant failure load using:

$$K_I = C\sigma\sqrt{\pi a} \tag{2}$$

where $\sigma$ is the fracture strength, $a$ is the crack length and $C$ is given by:

$$C = 1.12 - 0.231\left(\frac{a}{W}\right) + 10.55\left(\frac{a}{W}\right)^2 - 21.72\left(\frac{a}{W}\right)^3 + 30.39\left(\frac{a}{W}\right)^4 \tag{3}$$

where $W$ is the ribbon width.

The fracture surfaces of the wire and ribbon samples were examined by SEM operated at 20 kV.

## RESULTS AND DISCUSSION

### *Tensile strength and Vickers hardness*

Figure 3 shows the microhardness, $H_v$, and tensile strength, $\sigma_f$, for the $Fe_{78-x}Cr_xSi_{10}B_{12}$ alloy wires and HT steel wires. It can be seen that both $H_v$ and $\sigma_f$ increase with increasing Cr content. These increases in $H_v$ and $\sigma_f$ are broadly consistent with those observed previously [3] for the $Fe_{75-x}Cr_xSi_{10}B_{15}$ alloy series, although the absolute values are significantly smaller, consistent with the lower B content in the present case. The Cr containing alloy wires proved to be easier to cast with a uniform cross section than the $Fe_{78}Si_{10}B_{12}$ base alloys because, it is considered, of the formation of a surface film of Cr/Si hydrated oxide (confirmed by XPS studies [3,5]), which aided in stabilising the liquid jet. The $Fe_{78}Si_{10}B_{12}$ wire was subsequently characterised by a shallow necking which could adversely influence the measured strength and fatigue life.

The fracture toughness, $K_I$, for $Fe_{78-x}Cr_xSi_{10}B_{12}$ system is almost constant over the range of Cr content (Figure 4). The values are similar to those reported for NiCrB glassy ribbon and X-200 steel [7]. Fracture in both wires and ribbons occurred by shear-induced deformation following inhomogeneous flow, similar to previously reported fractures in these glassy alloys [7-9]. The fracture occurred at ~45° to the tensile axis (i.e. plane of maximum critical resolved shear stress), implying that fracture was shear induced. The fracture morphologies for wires and ribbons consisted of two distinctive regions; one uniform, and the other veined, as has been reported previously [9-11], (figure 5). The smooth regions represent the initial shear displacement. The fracture veins resulted from the existence of a “liquid-like” or softened layer formed during shear displacement, involving extensive plastic flow, corresponding to instability phenomena characteristic of ductile glassy alloys [8]. It has been suggested [10] that the thin layer of softened material must result from local heating occurring under close to adiabatic conditions. The fracture morphology in the

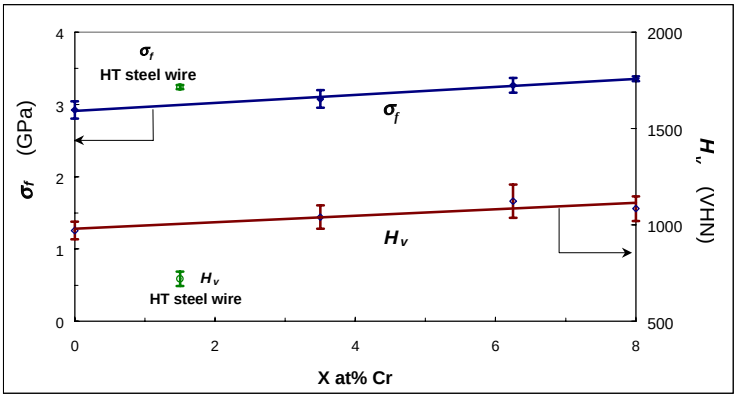


**Figure 3.- Tensile strength and Vickers microhardness results for the $Fe_{78-x}Cr_xSi_{10}B_{12}$ wires tested.**

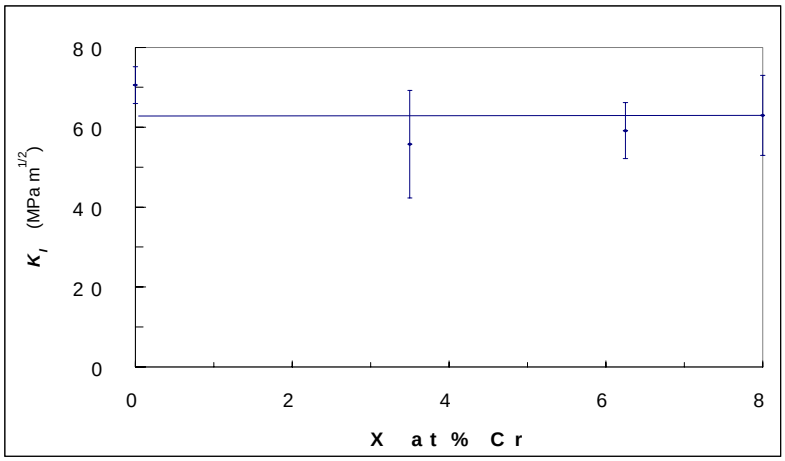


**Figure 4.- Fracture Toughness, $K_I$ results on $Fe_{78-x}Cr_xSi_{10}B_{12}$ ribbons.**

HT steel wire was characteristic of this type of high strength steel.

***Fatigue***

The fatigue performance of these wires is shown in figure 6. It can be seen that, in general, increasing the Cr content leads to improved fatigue performance, especially under high cycle conditions. In particular, there is a noticeable difference in performance between the 0 and 3.5 at% Cr samples and the 6.25 and 8 at% Cr samples; corrosion pits, that could act as crack nucleating sites were observed for both the 0 and 3.5 at% Cr alloys. This is in line with previously reported enhancements in the fatigue performance of $Fe_{77.5-x}Cr_xSi_{7.5}B_{15}$ and $Fe_{75-x}Cr_xSi_{10}B_{15}$ amorphous alloys with increasing Cr content [3-5].

Previous studies [3-5] have shown that the initiation of the fatigue crack is environmentally dependent. The presence of corrosion pits at fracture initiation sites observed in the present study lends support to this conclusion. In addition, wire smoothness is expected to play an important role; alloys with 0 and 3.5 at% Cr showed periodic shallow necking along their lengths, leading to stress concentrations and premature fatigue failure. Olofinjana and Davies [3] suggested that the enhancement of fatigue strength due to Cr addition could not be attributed to the effect of the Cr on the intrinsic mechanical properties alone, since the fatigue life does not scale with the static strength, whose increase with Cr content is relatively modest. It was assumed [3,4] that fatigue life enhancement is probably largely due to a surface phenomenon and that fatigue crack initiation is suppressed by a Cr rich film. XPS studies [3,5] demonstrated that the spontaneous formation of a passive thin film formed of a Cr/Si hydrated oxide on the outside surface of the wires appeared to accelerate the improvement of fatigue strength through the enhancement of corrosion resistance. No change occurred in microhardness for any of the wires tested, which suggests that there was no softening or hardening during the process of fatigue.

Fatigue experiments with $\sigma_m$ = 200 and 900 and 1550 MPa were carried out on the DP machine only since tensioning load stresses of 900 MPa or lower could not be used in the SP machine. In contrast, the DP

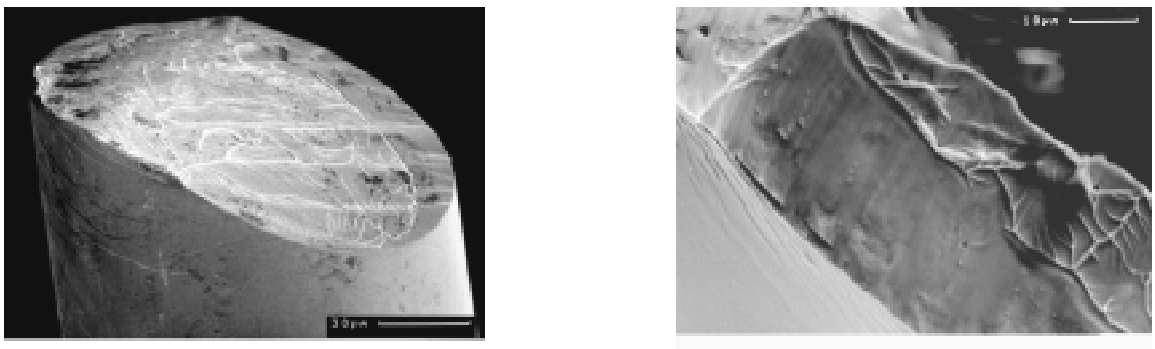

**(a)** **(b)**

**Figure 5.- Tensile fracture morphologies for (a) wire and (b) ribbon amorphous alloys.**

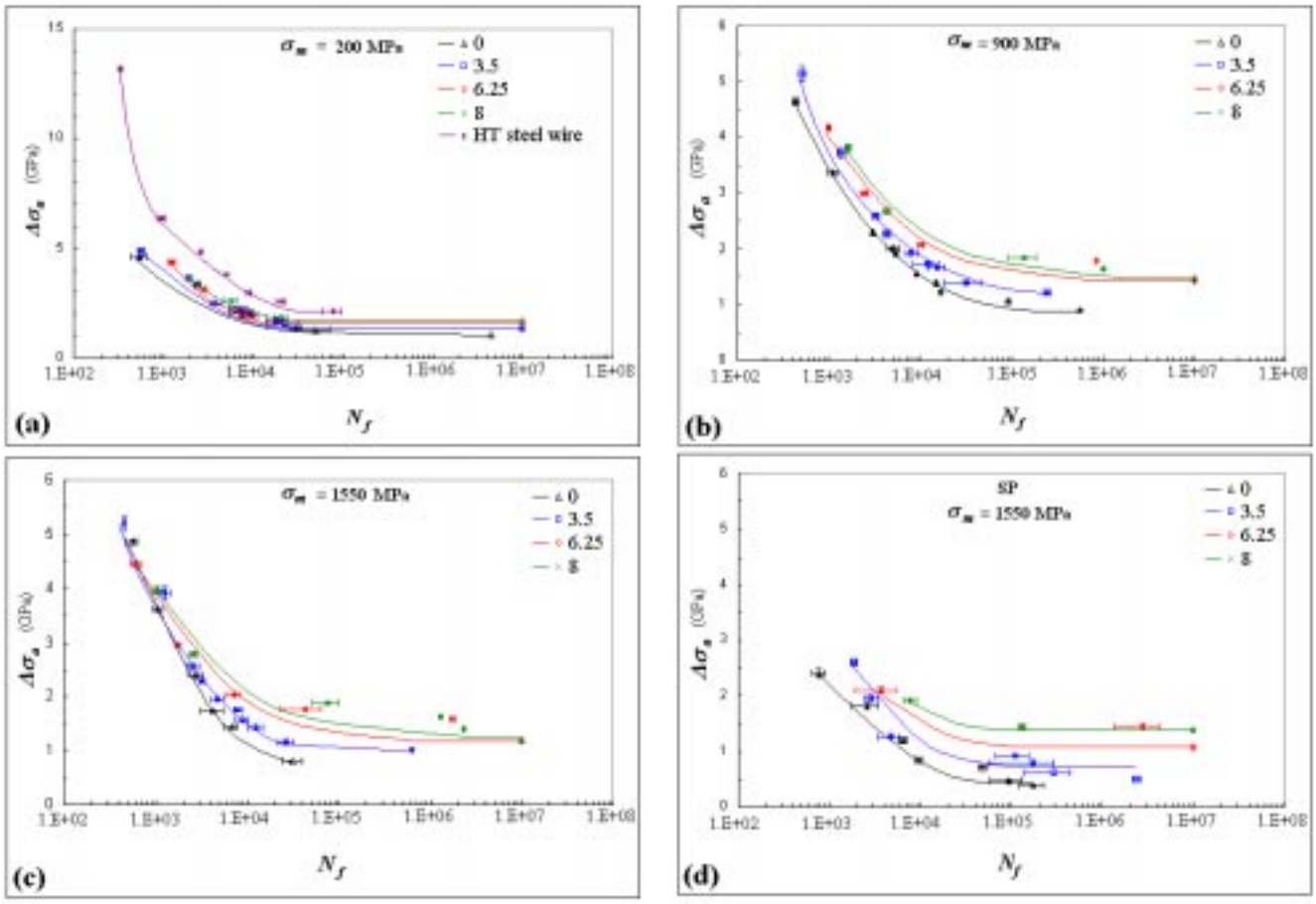


**Figure 6.- Fatigue results for $Fe_{78-x}Cr_xSi_{10}B_{12}$ glassy and HT steel wires tested in function of stress.**

machine can be operated with $\sigma_m$ as low as 150 MPa. Figure 6 also shows the maximum number of cycles reached for each alloy wire.

Although the DP machine can produce tension/compression loading, in practice, only the glassy wires tested at $\sigma_m$ = 200 MPa in the DP machine were subjected to tension/compression loading for all the stress ranges used. Under high mean stress conditions ($\sigma_m$ = 900 and 1550 MPa), the wires were subjected to tension/compression stress for large stress ranges (low cycle fatigue), but only tension/tension loading for low values of the stress range (figure 2.a).

Figure 6.(a) suggests that HT steel wires have superior fatigue performance to the amorphous alloy wires. In terms of stress this is correct; however, higher stresses are generated in HT steel wires for a given strain because of the higher modulus of HT steel compared to the amorphous alloys. Thus, if the data are reported in terms of strain range, the amorphous alloy wires have generally similar performance to HT steel wires (see figure 7).

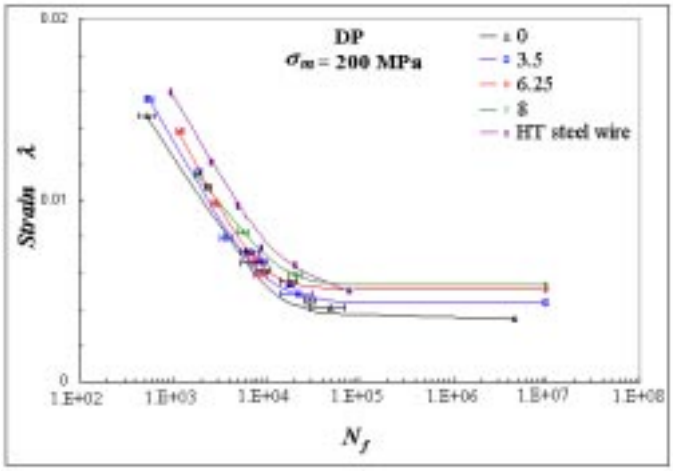


**Figure 7.- Fatigue results for $Fe_{78-x}Cr_xSi_{10}B_{12}$ glassy and HT steel wires tested in function of strain.**

Fractographic studies of the amorphous wires indicate that similar fracture surfaces are obtained on samples tested in the SP machine and in the DP machine if the samples tested in the DP machine were only subjected to tension/tension loading (high mean stress, low stress range conditions). In this case a relatively rough region surrounds the crack initiation site which develops at a shear displacement. This rough region is believed to be due to repeated shear events during the cyclic loading process. Surrounding this relatively rough region of fatigue crack growth is a smoother region which becomes progressively rougher on moving further away from the crack initiation site. This is believed to be the region of fast fracture.

For larger stress ranges in the DP machine where the samples are significantly rougher, (see figure 8). In this case, there is no clear evidence of a single fracture emanating from a region of cyclic crack growth. This is because two opposing regions of the wire see tensile stress whereas in tension/tension loading one region of the wire sees tensile stresses (which lead to cyclic crack growth and eventual failure) whereas the opposing region only sees compressive stress. Thus, in the tension/compression case, fatigue cracking can emanate from two different regions of the wire and, judging by the shear events visible on the exterior surface of the wire, may potentially start from several points within those regions. However, as a fatigue crack becomes dominant on one side of the wire the stress across the remaining section of the wire in the vicinity of crack is increased and thus a growth of nearby fatigue crack on the other side of the wire will be enhanced. As a result, the final fracture may be due to the interception of at least two fatigue cracks growing separately from each other, but whose growth enhances the stresses on the other crack. In this case, as most of the fracture is due to fatigue crack growth, the entire fracture surface is very rough (Figure 8). Of course, a fatigue crack may not initiate at similar points on the two sides of the wire. In this case, one crack will tend to dominate and a situation such as that shown in figure 9 is observed. The precise features are related to the number of shear events generated which depends on the stress range used.

*Large stress range* (low cycle).- Large numbers of shear bands are generated on the surfaces of wires subjected to the tensile and compressive bending stresses. The potential for the nucleation of cracks on these shear bands is high; the fatigue crack would be expected to initiate at the root of one or more shear steps after an incubation period. Figure 8.b shows evidence that there were at least two cracks initiated for fracture, resulting in 100% ductile failure.

*Medium stress range* (medium cycle).- The bending stresses generate a few shear bands. The process of crack initiation could occur in a manner similar to that suggested by Inoue *et al* [12]: (a) the glassy wire usually contains a rather high residual stress. (b) repetitive bending load generates shear steps in the high tensile residual stress region on the wire surface. (c) a small corrosion pit generates at the shear event in a high surface energy state. (d) the adsorption and dissociation of moisture in air become easier near the corrosion pit, resulting in the generation and dissolution of hydrogen. The increases of internal stress and embrittlement sensivity due to the dissolution of H give rise to easy initiation and propagation of the fatigue crack, leading to final fracture. The diffusion of H down the shear band would be accelerated by the additional free volume generated by the shear event [3]. The ductile fracture, i.e. from crack initiation to the initiation of the brittle fracture extends to 50 to 80 % of the sample diameter.

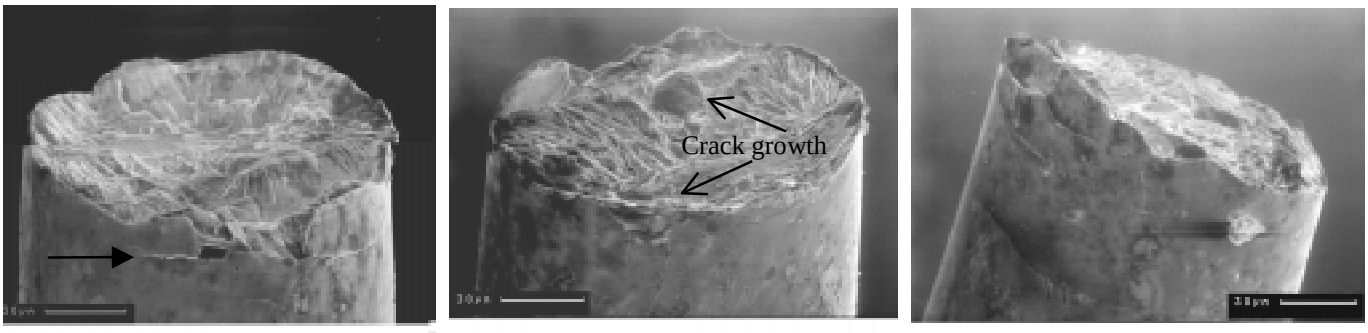


**(a)** **(b)** **(c)**

**Figure 8.- Fracture morphology of $Fe_{74.5}Cr_{3.5}Si_{10}B_{12}$ glassy wire tested in the DP machine, failed at $\Delta\sigma_\alpha$ = 5.42 GPa, using $\sigma_m$ = 900 MPa.**

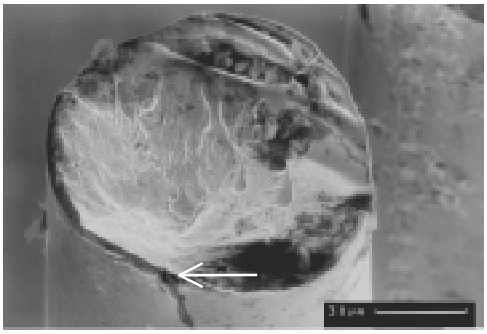

**Figure 9.- $Fe_{61.75}Cr_{6.25}Si_{10}B_{12}$ glassy wire fractured in the DP fatigue machine at 2132 cycles applying $\Delta\sigma_a$ = 3.34 GPa, using $\sigma_a$ = 200 MPa.**

*Low stress range* (high cycle).- Here, the mechanism of fracture is similar to that for the medium stress range. The difference is that the fraction of rough length is between 15 and 50 % of the sample diameter, see figure 10.

The occurrence of pitting corrosion would only be expected for alloys with 0 and 3.5 at% Cr. For the alloys with 6.25 and 8 at% no pitting corrosion was found at any of the points of crack initiation for medium and high cyclic stresses. Thus, in this case, a fatigue crack is initiated at the root of a shear step after a long incubation period. The fraction of rough length from the crack initiation to fracture is approximately 15 %, (figure 11). Fracture in HT steel wire initiated at shear bands generated on both surfaces of the wire. The initial morphology of the fracture was smooth with small peaks of about 3 μm. The final part of the fracture was ductile, characteristic of crystalline wires (figure 12).

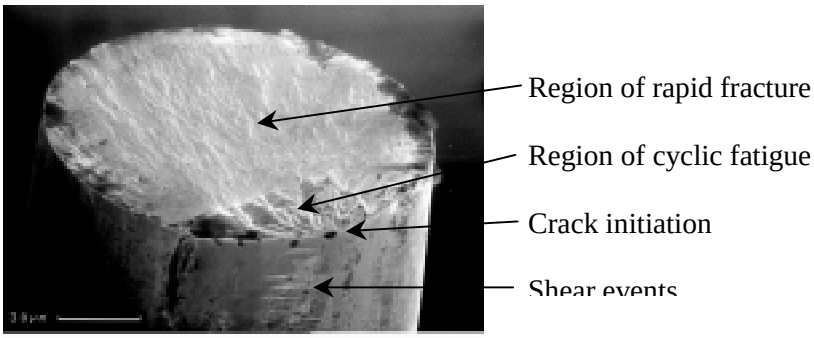


**Figure 10.- Fatigue fracture for $Fe_{73.5}Cr_{3.5}Si_{10}B_{12}$.**

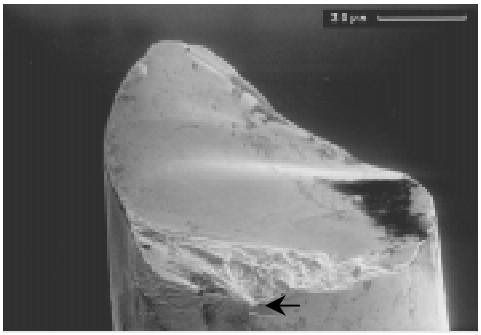

**Figure 11 .- $Fe_{61.75}Cr_{6.25}Si_{10}B_{12}$ glassy wire. fractured in the DP machine.**

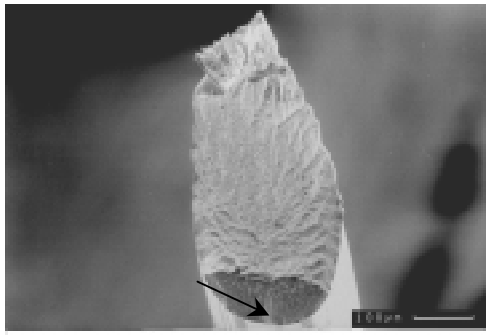

**Figure 12.- HT steel wire fractured in the DP machine.**

## CONCLUSIONS

Only compressive to tensile bending stresses in the DP machine were performed at $\sigma_m$ = 200 MPa for all stress ranges used. Under high cycle conditions at $\sigma_m$ = 900 and 1550 MPa, the machine imparts bending stresses similar to the SP machine.

$Fe_{70}Cr_8Si_{10}B_{12}$ glassy alloy wire yielded the highest fatigue strength for both fatigue bending machines at all $\sigma_m$ values used.

Fracture morphologies in the SP machine were similar to those obtained previously, with a region of fatigue crack growth followed by fast fracture. Fracture morphologies in the DP machine at large stress ranges were different from those obtained with the SP machine but similar for low stress ranges. Fractures were similar for the four glassy alloy compositions studied and for all $\sigma_m$ values, with cracks initiating at shear events. Fractures obtained in the medium and low stress ranges resulted from the nucleation of cracks at corrosion pits formed on surface shear steps for the alloys containing 0 and 3.5 at% Cr.

## ACKNOWLEDGEMENTS

One of us, Jorge Verduzco, would like to acknowledge the financial support received from CONACyT, México.

## REFERENCES:

1.- Onhaka, I. (1984-85) *Int. J. of Rap. Sol.,* **4**, 219.
2.- Hagiwara, M., Inoue, A. and Masumoto, T. (1982) *Met. Trans.* **13A**, 373.
3.- Olofinjana, A. and Davies, H. A. (1994) *Mater. Sci. and Engng.* **A186**, 143.
4.- Hagiwara, M., Inoue, A. and Masumoto, T. (1985). In *Rap. Quench. Met.,* pp. 1779-1782, Steeb, S. and Warlmont, H. (Eds.), Elsevier Science Publishers, New York.
5.- Olofinjana, A., Nurminen, J. and Davies, H. A. (1994). In *Proceedings of the Fourth International Workshop on Non-Crystalline Solids*, pp. 72-78, Vázquez, M. and Hernando, A. (Eds.), Madrid, Esp.
6.- Donald, I. W., Whang, S. H., Davies, H. A. and Giessen, B. C. (1981). In *Proceedings of the 4th International Conference on Rapidly Quenched Metals*, pp. 1377-1380, Sendai.
7.- Masumoto, T. and Maddin, R. (1975) *Mater. Sci. and Engng.* **19**, 1.
8.- Spaepen, F. and. Taub, A. I (1983). In *Amorphous Metallic Alloys*, pp 231-255, Luborsky, F. E Editor. Butterworths, London.
9.- Olofinjana, A. and Davies, H. A. (1994) *Int. J. of Rap. Sol.* **8**, 225.
10.- Spaepen, F. (1975) *Acta Met.* **23**, 615.
11.- Hagiwara, M., Inoue, A. and Masumoto, T. (1982) *Mater. Sci. and Engng.* **54**, 197.
12.- Inoue, A., Hagiwara, M. and Masumoto, T. (1988) *Sci. Rep. RITU, Series A* **34**,48.